A Mouse Bone Marrow Dosimetry Model

Moorthy S. Muthuswamy, Peter L. Roberson and Donald J. Buchsbaum
Department of Radiation Oncology, University of Michigan, Ann Arbor, Michigan; and Department of Radiation Oncology, University of Alabama, Birmingham, Alabama

Bone marrow is the primary dose-limiting organ in radioimmunotherapy. Athymic nude mouse models are used to guide radioimmunotherapy in humans. In the mouse, the dimensions of the marrow are comparable to the mean range of the beta particles for a wide variety of beta-emitting radionuclides, so local beta energy deposition cannot be assumed. **Methods:** We have developed a computer simulation model in which slab, spherical and cylindrical geometries of the bone marrow of the mouse were incorporated. The energy deposition within the marrow was estimated using beta dose point kernels for several beta-emitting radionuclides. **Results:** The calculated percentages of energy deposited in the mouse marrow using the full geometry were 46%, 24% and 10% for ^{131}I-, ^{186}Re- and ^{90}Y-radiolabeled antibodies, respectively. Assuming a concentration of activity in the marrow of 0.36 times the blood activity concentration, the percentages of energy deposition in the marrow from marrow and whole-body sources were 61%, 40% and 29% for ^{131}I, ^{186}Re and ^{90}Y, respectively. **Conclusion:** This work shows that, even for the lower mean beta energy-emitting radionuclide, such as ^{131}I, accurate computation of the mouse bone marrow dose involves including both the energy loss from beta decays within the marrow and dose contributions from tissue surrounding the marrow.

Key Words: mouse models; bone marrow; dose kernels; dosimetry; computer simulation

J Nucl Med 1998; 39:1243–1247

With bone marrow as the dose-limiting tissue, it becomes useful to calculate tumor dose normalized to bone marrow dose when comparing radioimmunotherapy dosimetry for different radionuclides (*1*). A model was developed by Hui et al. (*2*) for ^{90}Y mouse bone marrow dosimetry that does not assume local energy deposition of beta particles that are emitted inside the marrow. This model also computed the dose to marrow from the rest of the mouse body. Recently, Behr et al. (*3*) went a step further by incorporating the actual mouse anatomy as represented by MRI with a three-dimensional internal dosimetry package developed by Sgouros et al. (*4*) and estimated the bone marrow dose for ^{90}Y-radiolabeled antibodies. With the dimensions of the mouse marrow (*5,6*) comparable to the mean energy range (Table 1) of the beta radiation, the significance of the assumption of local beta energy deposition becomes important. The mean energy range (*7,8*) in Table 1 is defined as representing the range of 60% of the tissue energy deposition distribution. About 47%, 20%, 21% and 12% of the bone marrow in the mouse are in ribs, limbs, vertebrae and skull, respectively (*5,6*). The Hui et al. (*2*) model used beta dose point kernels that were convolved with the activity distributions inside the marrow to arrive at the fraction of the beta energy deposited within the marrow, but in the Hui model, only the fraction of the mouse bone marrow in the limbs was considered. In the case of the mouse, all of the marrow may be active (*9*); hence, it is relevant to take all of the marrow into consideration. Furthermore, it is of interest to compute mouse bone marrow dose for ^{131}I and ^{186}Re, which have different mean energy ranges from that of ^{90}Y (Table 1).

Compared to our earlier work (*1*), the significant change in the current work is that we have incorporated more components of mouse marrow. In the earlier work (*1*), the bone marrow activity concentration to blood activity concentration ratio of 0.18 was used. In this work, a more realistic activity concentration ratio of 0.36 was used. Also in the earlier calculation (*1*), dose point kernels (*10*) of the radionuclides were not used. Instead, X_{60}, the less accurate mean energy range (Table 1) approach was used for the radionuclides. In the mean energy range approach used previously (*1*), the radionuclide was assumed to lose energy constantly before it came to a stop at the mean energy range. However, the dose point kernels plotted in Figure 1 show a shape of energy loss that is not constant as a function of distance. The dose point kernels represent the probability distribution of the radionuclide energy deposition distribution as a function of the scaled distance. The kernel is normalized in such a way that its integration over the scaled distance is unity. Here, the scaled distance times the continuous slowing-down approximation (CSDA) (*10*) range gives the actual distance.

The beta dose point kernels (*10*) of ^{131}I, ^{186}Re and ^{90}Y radionuclides were integrated to obtain the dose deposited within the marrow volume from the activity within the marrow. Only that part of the beta particle energy deposited within the bone marrow geometry was taken to contribute toward its dose. The contribution of the activity in the rest of the mouse to the bone marrow dose was also calculated to arrive at the total marrow dose. Quantitative comparisons of human marrow and mouse marrow dose deposition of these radionuclides are also discussed.

MATERIALS AND METHODS

In Table 2, the geometries of various bone marrow sites of a mouse and the percentage contributions are listed (*5,6*). In the case of limbs, we have assumed a cylindrical geometry 2 cm long. The purpose here is to compute the mean energy deposited by a beta particle for these different geometries. The beta particle is assumed to be emitted in a random direction and from anywhere within the geometry. A Monte Carlo algorithm that uses a random generator was used to randomly choose the direction of emission of a beta particle. The dose point kernel appropriate for the radionuclide was integrated for the scaled (normalized to the CSDA) track length within the marrow geometry to compute the fractional energy deposited within the marrow. All integration calculations appearing in this report were performed by numerical summation.

Spherical Geometry

The methodology was to increment the radial location of the beta particle emission (r_i) from zero to the length of the radius of the sphere (r_{sph}) and randomize the emission angle (θ) of the beta ray (Fig. 2). In this spherical geometry, the number of points at a distance r_i from the center is proportional to $4\pi r_i^2$. Also, there is an increase in the number of azimuthal orientations with θ that is

Received Apr. 1, 1997; revision accepted Oct. 15, 1997.
For correspondence or reprints contact: Moorthy S. Muthuswamy, PhD, Department of Radiation Oncology, Mount Sinai Hospital, 1 Gustave L. Levy Pl., New York, NY 10029.

TABLE 1
Radionuclide Properties

	Radionuclide		
	^{131}I	^{186}Re	^{90}Y
Mean energy (keV)	182	349	938
CSDA range (mm)	3.37	4.83	11.30
Range at mean energy (mm)	0.40	0.92	2.76

Data from References 8 and 10. CSDA = continuous slowing-down approximation.

proportional to $\sin\theta$. This gives a combined probability factor for each point of $4\pi r_l^2 \sin\theta$.

From Figure 2, the following equation was derived:

$$r_{sph}^2 = r_l^2 + s^2 + 2sr_l \cos\theta. \quad \text{Eq. 1}$$

This quadratic equation was solved for s, the distance a beta particle travels from the point of emission to the surface of the spherical geometry. Of the two possible solutions of the quadratic equation, the correct one was positive.

So, for each point r_l, the distance(s) a beta particle travels was computed from Equation 1 for the randomly chosen angle of emission. It was divided by the CSDA range to convert it in terms

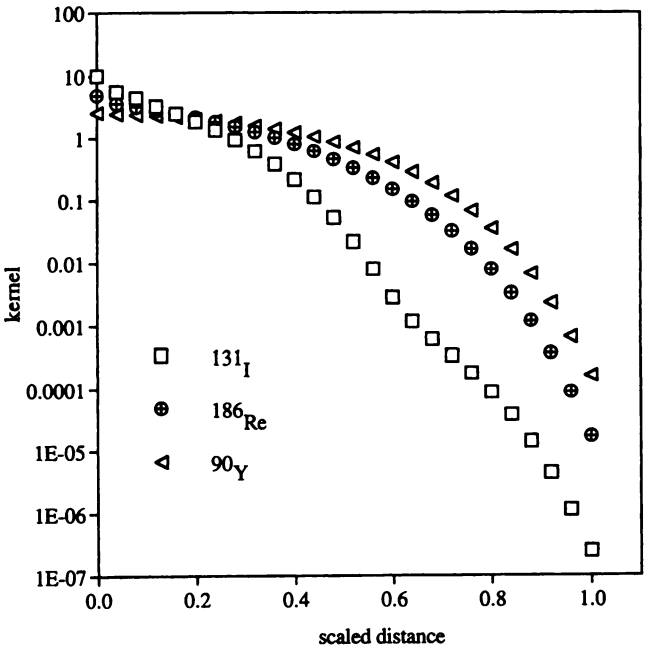

FIGURE 1. Dose point kernels (*10*) of ^{131}I, ^{186}Re and ^{90}Y radionuclides are plotted as a function of the scaled distance. The integral of the kernels over the scaled distance is normalized to unity. Actual distances are obtained by multiplying the scaled distances by the CSDA appropriate for the radionuclide.

TABLE 2
Geometry of Mouse Marrow

Components	% total	Model
Ribs, clavicle, sternum, pelvis	47	Slab: 300-μm thick
Limb bones	20	Cylinder: 900-μm diameter
Vertebrae (excluding tail)	21	Sphere: 200-μm diameter
Skull	12	Sphere: 170-μm diameter

Data from References 5 and 6.

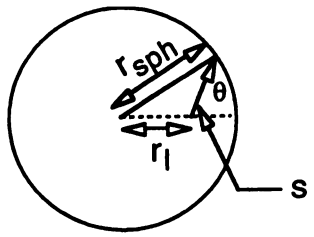

FIGURE 2. Spherical geometry of marrow cavities in vertebrae and skull. The point of emission of a beta particle was located at a distance r_l from the center of the sphere of radius (r_{sph}). The emission angle was θ. The distance from the emission point to the geometrical surface was s.

of the scaled length (l_s = s/CSDA range). The kernel appropriate for the radionuclide was integrated over the scaled length from 0 to s_{scale} (s_{scale} = r_{sph}/CSDA range) to arrive at the fraction of energy deposited for the beta particle track length of s inside the geometry. It was multiplied by the weight factor of $4\pi r_l^2 \sin\theta$ for the location r_l and the emission angle θ. This procedure was repeated for all ranges of the variables ($0 \le r_l \le r_{sph}$ and $0 \le \theta \le 180$), and the result was integrated. Finally, the integrated result was divided by an overall normalization factor that is the integration without the kernels. Mathematically, the expression for the fraction of the energy deposited (f) is as follows, with $l_s(r_l,\theta)$ as the scaled length and $K(l_s)$ as the kernel:

$$f = \frac{\int_{r=0}^{r_{sph}} \int_{\theta=0}^{\pi} 4\pi r^2 \sin\theta \int_{l_s=0}^{s_{scale}} K(l_s(r,\theta))\, dl_s\, dr\, d\theta}{\int_{r=0}^{r_{sph}} \int_{\theta=0}^{\pi} 4\pi r^2 \sin\theta\, dr\, d\theta}. \quad \text{Eq. 2}$$

Cylindrical Geometry

For this geometry, there are two emission angles associated with a beta particle (polar angle $0 \le \theta \le 180$; azimuthal angle $0 \le \phi \le 180$) (Fig. 3). The projection of a beta ray in the circular plane of the cylinder was $s \cdot \sin\theta$. The emission angle in that plane was ϕ. In this cylindrical geometry, the number of points at a distance r_l from the center is proportional to $2\pi r_l$. Also, there is an increase in the number of azimuthal orientations with θ that is proportional to $\sin\theta$. This gives a combined probability factor for each point of $2\pi r_l \sin\theta$. From the geometry in Figure 3:

$$r_{cyl}^2 = (r_l + s \cdot \sin\theta \cos\phi)^2 + (s \cdot \sin\theta \sin\phi)^2. \quad \text{Eq. 3}$$

Sampling was performed both radially and vertically. Due to the vertical symmetry, only the upper half of the cylinder was sampled. Also, due to the azimuthal symmetry of the half-circle of the cylinder, the azimuthal angle was sampled only up to 180°. In addition, the finite length of the cylinder was considered when calculating the length of the beta particle track within the cylindrical geometry. When a beta particle track passed through the ends

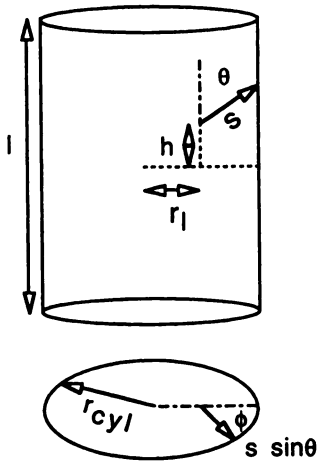

FIGURE 3. Cylindrical geometry of marrow cavities in limb bones. The point of emission of a beta particle was located at a radial distance r_l from the cylindrical (of radius r_{cyl}) axis. The point was also located at a distance (h) from the midpoint of the cylinder along its axis. The polar emission angle was θ. The distance from the emission point to the geometrical surface was s. The projection of the distance s on the circular plane was $s \cdot \sin\theta$, with an azimuthal emission angle of ϕ.

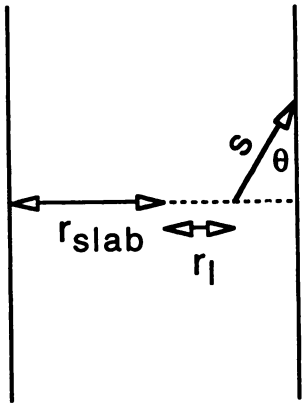

FIGURE 4. Slab geometry of marrow cavities in ribs, clavicle, sternum and pelvis. The point of emission of a beta particle was located at a distance r_l from the slab center. The emission angle was θ. The distance from the emission point to the geometrical surface was s. The half-thickness of the slab was r_{slab}.

of the cylinder, s was adjusted as $(1 \cdot 0.5 - |\sec\theta| \cdot h/\sec\theta) \cdot |\sec\theta|$, where l was the length of the cylinder and h was the vertical height of the emission point from the center of the cylinder. The expression for the fraction of energy deposited inside the cylindrical geometry, f, is (where $s_{scale} = r_{cyl}/\text{CSDA range}$):

$$f = \frac{\int_{h=0}^{l}\int_{\phi=0}^{\pi}\int_{r=0}^{r_{cyl}}\int_{\theta=0}^{\pi} 2\pi r \sin\theta \int_{l_s=0}^{s_{scale}} K(l_s(r,\theta,\phi,h))dl_s dr d\theta d\phi dh}{\int_{h=0}^{l}\int_{\phi=0}^{\pi}\int_{r=0}^{r_{cyl}}\int_{\theta=0}^{\pi} 2\pi r \sin\theta dr d\theta d\phi dh}. \quad \text{Eq. 4}$$

Slab Geometry

From Figure 4, the following equations were derived:

$$s = \frac{r_{slab} - r_l}{\cos\theta} \qquad 0 \le \theta \le 90. \qquad \text{Eq. 5}$$

$$s = \frac{r_{slab} + r_l}{\cos(180 - \theta)} \qquad 90 \le \theta \le 180. \qquad \text{Eq. 6}$$

The variable r_l was sampled from 0 to r_{slab}. The probability factor associated with the angle of emission was $\sin\theta$. As before, the fraction of energy deposited within the slab volume is given by f (where $s_{scale} = r_{slab}/\text{CSDA range}$):

$$f = \frac{\int_{r=0}^{r_{slab}}\int_{=0}^{\pi} \sin\theta \int_{l_s=0}^{s_{scale}} K(l_s(r,\theta))dl_s dr d\theta}{\int_{r=0}^{r_{slab}}\int_{\theta=0}^{\pi} \sin\theta dr d\theta}. \qquad \text{Eq. 7}$$

For each of the above geometries the fraction of the energy deposited was computed for the radionuclides listed in Table 1. By weighting the absorbed fractions by the percentage of the total bone marrow (Table 2), the total absorbed fractions in mouse bone marrow was computed. The expression used for the total fraction (P) computation was:

$$P = 0.47f_r + 0.20f_l + 0.21f_v + 0.12f_s \qquad \text{Eq. 8}$$

Here, f_r, f_l, f_v and f_s are the fractional energy deposited in ribs, limbs, vertebrae body and skull, respectively.

The dose to the mouse marrow has contributions from the rest of the body. The injected activity in blood was assumed to be dispersed throughout the body. There is a wide variation (0.2–0.4) in the marrow-to-blood activity concentration ratios (*11*). However, recently, Sgouros (*12*) pointed out that the optimal value for this ratio is 0.36 for most types of antibodies used in radioimmunotherapy. Therefore, we assumed an activity concentration in bone marrow in mouse to be 0.36 times the activity concentration in blood. The ratio of the blood mass to the body mass for the human (*13*) was assumed to be 5400/70,000. The mouse blood mass to its body mass is similar (*14*). From the above information, the ratio of activity concentration between the bone marrow and the whole body for mouse was calculated to be 4.7. The percentage dose deposited in the bone marrow, including the whole-body contribution, was given by:

$$\%\ \text{total dose} = \left(\frac{(a_{BM} - a_{WB})P + a_{WB}}{a_{BM}}\right) 100. \qquad \text{Eq. 9}$$

Here, a_{BM} and a_{WB} are the activity concentrations in bone marrow and the whole body, respectively, and P is the total fractional dose (Eq. 8) deposited (self-dose) from the activity residing in the marrow averaged over all of the marrow geometries. The factor a_{WB}/a_{BM} is the fractional dose contribution to the marrow from the whole body. The rest of the fraction is due to the self-dose of excess activity in the marrow. Similar computations for any other radionuclide can be performed easily within this framework by incorporating the appropriate dose point kernels.

TABLE 3
Percentage Self-Energy Deposition in Various Components of Mouse Marrow

	Radionuclide		
	^{131}I	^{186}Re	^{90}Y
Ribs, clavicle, sternum, pelvis	57	33	14
Limb bones	65	37	12
Vertebrae	19	7.3	1.7
Skull	16	6.2	1.4
Average	46	24	10

RESULTS

The calculated percentages (Table 3) of self-energy deposited (P) in the bone marrow using the full geometry and weighting factors (Eq. 8) were 46%, 24% and 10% for ^{131}I, ^{186}Re and ^{90}Y, respectively. The calculated percentages of energy deposited in the marrow, including the contribution due to the activity in the rest of the mouse and using Equation 9, yielded 58%, 40% and 29% for ^{131}I, ^{186}Re and ^{90}Y, respectively. Including the gamma contributions to the mouse marrow computed in the next two paragraphs, the percentages were 61%, 40% and 29% for ^{131}I, ^{186}Re and ^{90}Y, respectively.

Assuming local energy deposition of the beta rays for ^{131}I (mean energy of 0.182 MeV), the S-factor for an organ with a mass of 20 g (the mass of an average mouse) is 1.938×10^{-2} rad/μCi-hr. From MIRD pamphlet 11 (*13*), the S-factor for the human thyroid to thyroid (mass of 20 g) is 2.2×10^{-2} rad/μCi-hr, including both beta and gamma particle contributions. Therefore, the mouse whole-body gamma contribution S-factor for ^{131}I is 0.262×10^{-2} rad/μCi-hr. Assuming local energy deposition, the ^{131}I beta S-factor for the mouse marrow of mass 0.43 g (scaled from the mouse S-factor, 1.938×10^{-2} rad/μCi-hr by the ratio of mouse mass to its marrow mass) is 90.4×10^{-2} rad/μCi-hr. The ratio of activity in the mouse marrow to the activity in whole body is given by $0.36 \times 1500/5400$. Here, 0.36 is the ratio of marrow to blood activity concentration ratio (*12*), and the ratio 1500/5400 is the ratio of marrow mass to blood mass in humans [this was assumed to be similar to that in the mouse (*14*)]. The ratio of dose to the mouse marrow from the whole-body gamma contribution relative to the local beta energy deposition of the activity in the mouse marrow is obtained by multiplying the ratio of the gamma to the beta S-factors by the activity ratios defined above and is 2.9% for ^{131}I.

In the case of ^{186}Re, MIRD pamphlet 11 (*13*) does not list the S-factors, and so a corresponding calculation could not be performed. However, the ^{186}Re and ^{131}I S-factor ratios of gamma contributions, S(RM ← TB) and S(RM ← RM), for humans (*1*) are 0.161 and 0.163, respectively. This indicates only a slight dependence of the ratio of ^{186}Re and ^{131}I gamma contribution S-factor ratios on the organ mass. For the mouse marrow, we take the ^{186}Re S-factor for the whole-body gamma contribution to be 0.16 times the ^{131}I gamma S-factor (previous paragraph), i.e., $0.16 \times 0.262 \times 10^{-2}$ rad/μCi-hr. Assuming local energy deposition, the ^{186}Re (mean energy of 0.349 MeV) beta S-factor for the mouse marrow of mass 0.4 g is 173.5×10^{-2} rad/μCi-hr. The ratio of dose to mouse marrow from the whole-body gamma contribution relative to the local beta energy deposition of the activity in mouse marrow is 0.6% for ^{186}Re.

DISCUSSION

We estimated that there was no more than a 2% uncertainty in the results in Table 3 due to the finite sampling of the volume in the computer simulation. Therefore, this uncertainty can be taken to represent the statistical variation of the calculational method. The dose deposition in the mouse bone marrow was beta energy-dependent. A factor of more than 4 times the marrow self-energy deposition occurred for ^{131}I compared to ^{90}Y due to the shorter range of the beta particles (Table 1). The fractional dose from the rest of the body to the marrow (fraction = 1/4.7) was significant for ^{90}Y due to the longer range of beta (21% of the 29% total rays).

Two aspects of the model are important to compute mouse bone marrow dose accurately. The first is the ability to compute the self-energy fractional deposition. For a cylindrical geometry of 0.5-mm radius and 9-mm length, Hui et al. (*2*) estimated that 15% of the beta energy was deposited within the volume for ^{90}Y. Our model calculation for this specific geometry resulted in 13% beta energy deposition within this volume, and hence, it compared well with the result of Hui et al. (*2*)

The second aspect is the computation of the marrow dose from the activity outside of the marrow. In the Hui model (*2*), the measured ^{90}Y activities in various organs were used to compute the cross-organ dose to the marrow using the dose point kernels, whereas in our approach, we assumed the activity to be distributed throughout the body through blood and the activity concentration in the marrow to be 0.36 times the activity concentration in blood (*12*). Therefore, it would be interesting to compare the dose to the marrow from rest of the body for these two approaches.

The ratio of total absorbed dose in marrow to the self-absorbed dose in marrow from Table 4 of Beatty et al. (*15*) is 3.4 for ^{90}Y. Beatty et al. (*15*) used the method developed by Hui et al. (*2*) to compute dose. From our model (Eq. 9) this ratio was $[(4.7 - 1) \times 0.13 + 1]/(4.7 \times 0.13) = 2.4$. Beatty et al. (*15*) had used actual measured activity concentrations in various organs to compute the dose. This could partly explain the difference between these two results. If we had used the marrow to blood activity concentration ratio of 0.24 instead of 0.36, the computed ratio of total absorbed dose in the marrow to the self-absorbed dose in our model for ^{90}Y would be 3.2, closer to the value of 3.4 reported by Beatty et al. (*15*). The ratio 0.24 is listed in the report of Seigel et al. (*11*) as the marrow-to-blood activity concentration ratio in the mouse. Because the activity concentration ratio in marrow to blood varies from 0.2 to 0.4 (*11*) and perhaps more (*12*), the ratio of total dose to marrow to the self-absorbed dose predicted by our model is consistent with the results reported by Beatty et al. (*15*). This comparison also underscores the importance of measuring the activity concentrations in marrow and blood accurately for a specific antibody. This comparison was also more significant for ^{90}Y due to its longer range beta particle, for which the majority of the mouse marrow dose comes from the rest of the body. Therefore, ^{90}Y is a good benchmark radionuclide to test this aspect of the model. This consistent comparison between our results and those of Beatty et al. (*15*) also provided a stronger case for our results for the lower mean energy radionuclides (^{131}I and ^{186}Re). Even for ^{131}I, there was a 42% (the self-dose was 36% and the contribution from the rest of the mouse body was 21%) marrow dose increase arising from the contributions of radioactivity in the rest of the mouse.

These calculations demonstrate dosimetric differences for improved geometric assumptions. If the antibody used has an increased affinity (different biodistribution) for the bone marrow, in this work, it can be considered by changing the value for the ratio of a_{BM} and a_{WB} in Equation 9, but if the antibody has increased affinity for organs close to most of the mouse marrow, for a longer range beta particle, there would be an increased contribution to the marrow dose (*2*). The limitation of this work is that such a scenario is not incorporated. In the case of humans, due to the larger scale of body dimensions and the associated larger separation between various organs, this effect should be less significant. However, the consistency of our results and those of Beatty et al. (*15*) imply that reasonably accurate results can be obtained by computing the dose from the mean activity concentration in the whole body of the mouse to the bone marrow.

In our earlier publication (*1*), the dose to human bone marrow was computed using MIRD pamphlet 11 (*13*) for both beta and gamma rays. Using the approach and the S-factors outlined in the Appendix of Muthuswamy et al. (*1*), in the case of humans, relative to the local beta dose deposition (self-dose) of all of the activity in the marrow:

1. The fractional beta dose depositions of activity in the marrow were 80%, 71% and 64% for ^{131}I, ^{186}Re and ^{90}Y, respectively (compared to 46%, 24% and 10% for the mouse);
2. Including the beta contribution from the rest of the human body, the percentage fractions were 85%, 75% and 71% (compared to 58%, 40% and 29% for the mouse); and
3. In addition, including the gamma component, the percentage fractions were 111%, 77% and 71% (compared to 61%, 40% and 29% for the mouse), respectively, for ^{131}I, ^{186}Re and ^{90}Y (*1*).

For the above calculations, in the expression $A_{RM} = a(m_{RM}/m_B)A_B$, a = 0.36 was assumed to be consistent with the mouse calculations.

These results illustrate quantitatively, for the radionuclides studied, that:

1. The self beta fractional dose for the mouse marrow is significantly smaller than that for the human marrow due to the smaller mouse marrow dimensions;
2. Consequently, the percentage contributions of beta dose from the rest of the mouse to the marrow are more significant in the case of the mouse marrow than for human marrow; and
3. Due to the greater bulk of the human body, the ^{131}I gamma dose contributions to the human marrow is much more significant than it is to the mouse marrow.

Using Equation 9, the total beta percentage doses to the human marrow given the self-dose percentages of 80%, 71% and 64% (previous paragraph) were 84%, 77% and 72% for ^{131}I, ^{186}Re and ^{90}Y, respectively. This close comparison with the percentages in the previous paragraph of 85%, 75% and 71% for ^{131}I,

^{186}Re and ^{90}Y, respectively, also gives credibility to the approach outlined in Equation 9 to compute dose to the marrow from the rest of the body.

CONCLUSION

This work emphasizes the fact that, although for the longer range radionuclides such as ^{90}Y, it is critical that external contribution to the marrow dose be considered, it is significant for lower energy radionuclides as well. It was also found that incorporating more of the mouse marrow improves the completeness of the marrow dose computation.

ACKNOWLEDGMENTS

This work was funded in part by National Cancer Institute Grant CA44173.

REFERENCES

1. Muthuswamy MS, Roberson PL, Ten Haken RK, Buchsbaum DJ. A quantitative study of radionuclide characteristics for radioimmunotherapy from three-dimensional reconstructions using serial autoradiography. *Int J Radiat Oncol Biol Phys* 1996;35:165–172.
2. Hui TE, Fisher DR, Kuhn JA, et al. A mouse model for calculating cross organ beta doses for yttrium-90-labeled immunoconjugates. *Cancer* 1994;73:951–957.
3. Behr TM, Sgouros S, Sharkey RM, et al. Yttrium-90-dosimetry in nude mice requires accounting for cross organ radiation: evaluation of three dosimetric models in relation to observed biological effects [Abstract]. *J Nucl Med* 1996;37:102P–103P.
4. Sgouros G, Barest G, Thekkumthala J, et al. Treatment planning for internal radionuclide therapy: three-dimensional dosimetry for nonuniformly distributed radionuclides. *J Nucl Med* 1990;31:1884–1891.
5. Sinclair WK. The relative biological effectiveness of 22-Mevp x-rays, cobalt-60 gamma rays and 200-Kevp x-rays. *Radiat Res* 1962;16:369–383.
6. Sinclair WK. Radiobiological dosimetry. In: Attix FH, Roesch WC, Tochilin E, eds. *Radiation dosimetry*, vol 3. New York: Academic Press; 1966:617–676.
7. Loevinger R, Japha EM, Brownell GL. Discrete radioisotope sources. In: Hine G, Brownell G, eds. *Radiation dosimetry*. New York: Academic Press; 1956:693–799.
8. Wessels BW, Buchsbaum DJ. Dosimetry of radiolabeled antibodies. In: Smith AR, ed. *Medical radiology: radiation therapy physics*. New York: Springer Verlag; 1995:365–384.
9. Tavassoli M, Yoffey JM. *Bone marrow structure and function*. New York: Alan R. Liss; 1983.
10. Prestwich WV, Nunes J, Kwok CS. Beta point dose kernels for radionuclides of potential use in radioimmunotherapy. *J Nucl Med* 1989;30:1036–1046;1739–1740.
11. Siegel JA, Wessels BW, Watson EE, et al. Bone marrow dosimetry and toxicity for radioimmunotherapy. *Antibody Immunoconjug Radiopharm* 1990;3:213–233.
12. Sgouros G. Bone marrow dosimetry for radioimmunotherapy: theoretical considerations. *J Nucl Med* 1993;34:689–694.
13. Synder WS, Ford MR, Warner GG, Watson, SB. Absorbed dose per unit activity for selected radionuclides and organs. In: *Medical internal radiation dose (MIRD) pamphlet 11*. New York: Society of Nuclear Medicine; 1975.
14. Roscoe B. *Biology of the laboratory mouse*. New York: McGraw-Hill; 1966.
15. Beatty BG, Kuhn JA, Hui TE, Fisher DR, Williams LE, Beatty JD. Application of the cross-organ beta dose method for tissue dosimetry in tumor bearing mice treated with ^{90}Y-labeled immunoconjugate. *Cancer* 1994;73:958–965.